was displayed when the organs at risk were contoured using postoperative radiation treatment planning CT. Diagnostic CT images were not fused to the planning scans. In the remaining 5 patients, postoperative radiation treatment planning CT only was used for contouring of the organs at risk. The peritoneal cavity was defined as including the volume surrounding the small bowel loops out to the edge of the peritoneum. The boundaries included the abdominal wall anteriorly and anterolaterally, the retroperitoneal and deep pelvic muscles posterolaterally, and the great vessels, vertebral bodies, and sacrum posteriorly. The rectum and bladder were excluded from the peritoneal cavity volume. DVH parameters subjected to analysis included the mean doses to the small bowel loops, large bowel loop, and peritoneal cavity, and the volumes of these organs receiving more than 15, 30, 40, and 45 Gy (V15-V45).

Follow-up and evaluation of chronic GI complications

The patients were followed up by gynecologic and radiation oncologists on an outpatient basis every month in the first year, every 2 months in the second year, every 3 months in the third year, every 4 months in the fourth year, every 6 months in the fifth year, and annually thereafter until 10 years after treatment. We defined a chronic complication as a GI event that occurred more than 3 months after radiation therapy was started. The severity of the GI complication was classified according to the RTOG/European Organization for Research and Treatment of Cancer Late Radiation Morbidity Score. Toxicity data including the grade of GI complications were collected retrospectively through hospitalization and follow-up records.

Statistical analysis

Associations between selected DVH parameters (V15, V30, V40, V45, and mean dose) and the incidence of grade 2 or higher chronic GI complications were evaluated. The relationships between clinical or DVH parameters and the incidence of chronic GI complications were analyzed with the Mann-Whitney *U* test for quantitative variables and the Fisher exact test for categorical variables. The mean DVH parameters for the small bowel loops, large bowel loop, and peritoneal cavity of patients with and without GI complications were compared by Mann-Whitney *U* test. Receiver operating characteristics (ROC) curve analysis of each of the DVH parameters was performed to select the most relevant threshold for prediction of a grade 2 or higher chronic GI complication. The predictive value of a parameter was evaluated based on the area under the ROC curve (AUC). The AUC reflects the ability of the test to distinguish between patients with and without disease. The optimal threshold for each DVH parameter was defined as the point yielding the minimal value for $(1 - \text{sensitivity})^2 + (1 - \text{specificity})^2$, which is the point on the ROC curve closest to the upper left-hand corner (9). Multivariate analysis using Cox regression models was performed to identify risk factors associated with grade 2 or higher chronic GI complications. The actuarial incidence of GI complications was calculated with the Kaplan-Meier method and differences between groups were compared by log-rank test. A P value of $<.05$ or a 95% confidence interval not encompassing 1 was considered to be statistically significant. All statistical tests were 2-sided.

Results

The characteristics of the 97 patients are shown in Table 1. The median follow-up period from the start of radiation therapy was 43 months (range 4-111 months). None of the patients experienced a local or distant recurrence within 3 months. The Eastern Cooperative Oncology Group performance status was 0-1 for all patients. The median age of the patients was 51 years old (range 28-70 years old). Twenty-three patients (24%) had a history of smoking, with a median Brinkman index (number of cigarettes per day × smoking years) of 400 (range 100-1200). The median total dose of nedaplatin was 285 mg (range 30-375 mg). Ninety-two patients (95%) received the whole RT dose as planned (50 Gy), but 3 patients (3%) received only 46 Gy and 2 (2%) received 44 Gy because of neutropenia (4 patients) or patient refusal (1 patient). Eighty-one patients (84%) had grade 0-1, 6 (6%) had grade 2, and 10 (10%) had grade 3 chronic GI

Table 1 Patient and treatment characteristics

	No. (%)
Age (y)	
Mean	51
SD	±10
T-stage	
T1	53 (55)
T2	44 (45)
N-stage	
N0	64 (66)
N1	33 (34)
Histology	
SCC	71 (73)
Ad	24 (25)
Others	2 (2)
Smoking	
None	74 (76)
Yes	23 (24)
Diabetes	
None	94 (97)
Yes	3 (3)
Abdominopelvic surgery	
None	94 (97)
Yes	3 (3)
BMI (kg/m^2)	
Mean	21.6
SD	±3.8
RT total dose (Gy)	
50	92 (95)
46	3 (3)
44	2 (2)
RT technique	
2D	65 (67)
3D	32 (33)
Total nedaplatin (mg)	
Mean	274
SD	±52

Abbreviations: 2D = 2-dimensional; 3D = 3-dimensional; Ad = adenocarcinoma; BMI = body mass index; RT = radiation therapy; SCC = squamous cell carcinoma; SD = standard deviation.

Table 2 Univariate analysis (Mann-Whitney *U* test and Fisher exact test) for the development of grade 2 or higher chronic GI complications

Variable	Grade 0-1 No.	Grade 2-3 No.	*P* value
Age (y)			
<52	39	10	.294
≥52	42	6	
Total nedaplatin (mg)			
<285	39	8	.892
≥285	42	8	
T-stage			
T1	46	7	.338
T2	35	9	
N-stage			
N0	53	11	.798
N1	28	5	
Histology			
SCC	60	11	.660
Non-SCC	21	5	
RT total dose			
50 Gy	76	16	.308
<50 Gy	5	0	
RT technique			
2D	57	8	.133
3D	24	8	
Smoking			
None	66	8	.005
Yes	15	8	
BMI (kg/m^2)			
<22	43	14	.011
≥22	38	2	

Abbreviations: 2D = 2-dimensional; 3D = 3-dimensional; BMI = body mass index; GI = gastrointestinal; RT = radiation therapy; SCC = squamous cell carcinoma.

Table 3 Comparison of mean DVH parameters of the small bowel loops, large bowel loop, and peritoneal cavity in patients with and without chronic GI complications (Mann-Whitney *U* test)

	Overall	Grade 0-1	Grade 2-3	*P* value
		Small bowel loops		
		Mean volume ± SE (mL)		
V15	337 ± 15	299 ± 13	527 ± 37	<.001
V30	308 ± 13	273 ± 11	485 ± 29	<.001
V40	289 ± 13	255 ± 11	458 ± 27	<.001
V45	280 ± 12	247 ± 11	444 ± 26	<.001
		Mean dose (cGy ± SE)		
	3,523 ± 80	3,429 ± 86	3,994 ± 160	<.001
		Large bowel loop		
		Mean volume ± SE (mL)		
V15	241 ± 12	241 ± 12	239 ± 34	.730
V30	207 ± 10	210 ± 11	192 ± 23	.550
V40	183 ± 10	189 ± 11	156 ± 17	.331
V45	176 ± 9	182 ± 10	149 ± 16	.321
		Mean dose (cGy ± SE)		
	2,747 ± 62	2,768 ± 66	2,639 ± 174	.487
		Peritoneal cavity		
		Mean volume ± SE (mL)		
V15	1,151 ± 29	1,129 ± 32	1,262 ± 70	.111
V30	1,045 ± 25	1,027 ± 27	1,138 ± 64	.174
V40	974 ± 25	960 ± 27	1,049 ± 65	.336
V45	941 ± 24	927 ± 26	1,013 ± 65	.343
		Mean dose (cGy ± SE)		
	3,421 ± 47	3,387 ± 50	3,596 ± 122	.169

Abbreviations: DVH = dose-volume histogram; GI = gastrointestinal; SE = standard error; V15-45 = volume receiving more than respective dose.

complications. Of the 10 patients with grade 3 GI complications, 5 (5% of all patients) had small bowel obstruction requiring surgery.

The incidence of chronic GI complications was analyzed as a function of clinical factors. Because there were few patients with diabetes or a history of abdominopelvic surgery among the study population, we did not analyze these factors. The results of univariate analyses are shown in Table 2. Smoking habit and low body mass index (BMI; <22) were significantly associated with grade 2 or higher GI complications. The mean DVH parameters of the small bowel loops, large bowel loop, and peritoneal cavity of patients with and without GI complications are shown in Table 3. Patients with grade 2 or higher GI complications had significantly greater V15-V45 volumes in the small bowel loops than did those without GI complications ($P<.001$). The mean dose to the small bowel loops differed significantly for patients with and without GI complications (39.94 vs 34.29 Gy, $P<.001$). In contrast, none of the parameters for the large bowel loop or peritoneal cavity were significantly associated with GI complications.

ROC curve analysis was performed to select the most relevant parameter to identify predictors of grade 2 or higher chronic GI complications among DVH parameters for the small bowel loops. The results are shown in Table 4. Because AUCs for mean dose, V15, V30, V40, and V45 were 0.693, 0.909, 0.912, 0.921, and 0.890, respectively, indicating that V15-V45 have good accuracy for prediction of GI complications. Strong collinearity among V15-V45 was expected in multivariate

Table 4 ROC curve analysis for DVH parameters of small bowel loops in relation to grade 2 or higher chronic GI complications

	AUC	95% CI	Optimal threshold Value	Optimal threshold Sensitivity/specificity (%)
Mean dose	0.693	0.580-0.806	3600 cGy	62.5/62.5
V15	0.909	0.855-0.963	380 mL	93.8/82.1
V30	0.912	0.857-0.967	360 mL	93.8/82.1
V40	0.921	0.869-0.972	340 mL	87.5/87.2
V45	0.890	0.819-0.962	340 mL	87.5/85.1

Abbreviations: AUC = area under the ROC curve; CI = confidence interval; DVH = dose-volume histogram; GI = gastrointestinal; ROC = receiver operating characteristics; V15-45 = volume receiving more than respective dose.

Table 5 Multivariate analysis for the development of grade 2 or higher chronic GI complications

Variable	HR (95% CI)	*P* value
V40 of small bowel loops (mL)	1.012 (1.007-1.018)	<.001
BMI (<22 vs ≥22)	3.024 (0.585-15.622)	.187
Smoking (yes vs no)	3.103 (1.023-9.415)	.046

Abbreviations: BMI = body mass index; CI = confidence interval; GI = gastrointestinal; HR = hazard ratio; V40 = volume receiving more than 40 Gy.

analysis. Therefore, we used V40 of the small bowel loops in multivariate analysis because this parameter had the highest AUC value. The optimal threshold for V40 was 340 mL. Thus, multivariate analysis was performed with V40 of the small bowel loops and 2 other clinical parameters that were judged to be potential risk factors for chronic GI complications: BMI and smoking habit. Of these 3 parameters, V40 of the small bowel loops and smoking emerged as independent predictors of GI complications (Table 5).

The overall incidences of grade 2 or higher GI complications were 0% (0/39), 7% (2/29), and 48% (14/29) for patients with V40 values of <250 mL, 250-340 mL, and >340 mL, respectively. Thus, the overall incidence of grade 2 or higher GI complications increased in a volume-dependent manner. Therefore, we performed Kaplan-Meier estimates of the cumulative incidence curves for grade 2 or higher chronic GI complications stratified by V40 of the small bowel loops using the above intervals. The cumulative incidence curves for grade 2 or higher chronic GI complications stratified by V40 of the small bowel loops are shown in Fig. The 3-year cumulative incidences of grade 2 or higher GI complications were 0%, 8.4%, and 46.2% for patients with V40 values of <250 mL, 250-340 mL, and >340 mL, respectively, with a significantly higher risk for patients with V40 > 340 mL than for the other groups ($P<.001$).

Discussion

Several previous studies have introduced predictive factors potentially associated with chronic GI complications after RT for gynecologic malignancies employing several types of therapy (3, 10-14). These factors include total RT dose, RT dose per fraction, history of diabetes, acute toxicity, BMI, age, previous abdominopelvic surgery, and smoking. In our study, smoking and low BMI were identified by univariate analysis as predictors of GI complications. Moreover, the V15-V45 volumes and the mean dose of the small bowel loops all showed a significant association with chronic GI complications. In addition, multivariate analysis identified V40 of the small bowel loops and smoking as independent predictors of GI complications. To the best of our knowledge, ours is the first study to show that DVH parameters of the small bowel loops derived with an up-to-date approach are associated with chronic GI complications after postoperative concurrent chemoradiation therapy for cervical cancer.

We believe that our findings are important for the practice of the radiation oncology, because adverse events caused by radiation exposure, such as GI complications, may be relieved by using an appropriate radiation technique or a mechanical device such as a belly-board. Recently, intensity modulated radiation therapy (IMRT) has emerged as a sophisticated technique for treatment of tumor regions or areas at risk of recurrence, while sparing adjacent normal tissue from high-dose irradiation, including in patients with gynecological cancer treated with IMRT after radical hysterectomy (15-18).

Two methods for contouring the small bowel volume have been reported: one uses direct delineation of the individual loops, whereas the other bases delineation on the peritoneal cavity because the bowel may lie within this space at any time throughout the course of treatment (5). Because these methods have not been compared to determine which leads to better predictions of chronic complications of the small bowel, we established separate parameters for the irradiated volume of the small bowel loops and the peritoneal cavity to examine which parameters correlated with

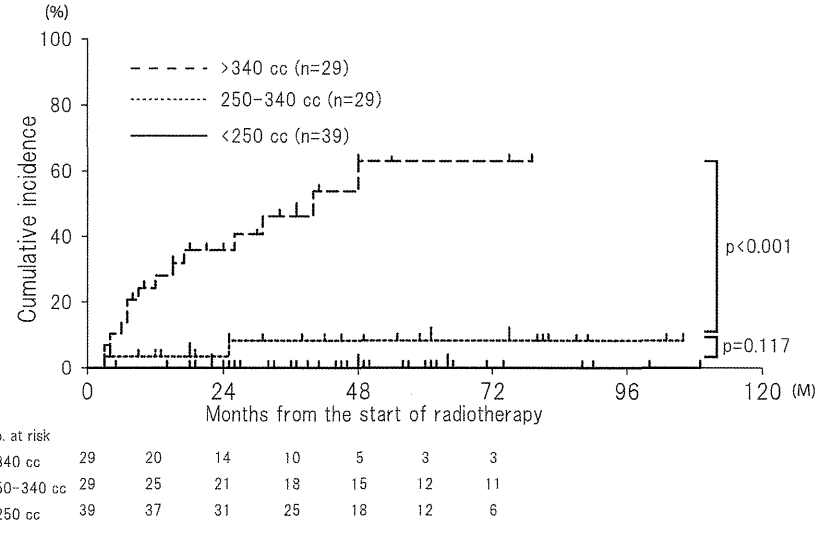

Fig. Kaplan-Meier estimates of cumulative incidence curves for grade 2 or higher chronic gastrointestinal (GI) complications stratified by V40 of the small bowel loops. The 3-year cumulative incidences of grade 2 or higher GI complications were 0%, 8.4%, and 46.2% for patients with V40 values of <250 mL, 250-340 mL, and >340 mL, respectively, with a significantly higher risk for patients with V40 > 340 mL than for the other groups (log-rank test; $P<.001$).

development of chronic GI complications. Interestingly, patients with grade 2 or higher chronic GI complications featured significantly higher V15-V45 volumes and mean dose to the small bowel loops than did patients without this feature. In contrast, none of the parameters for the peritoneal cavity showed any association with chronic GI complications. Similarly, parameters for the large bowel did not correlate with radiation-induced chronic GI complications. These findings suggest that, compared to the peritoneal cavity, the small bowel loops may constitute a better predictor of chronic GI complications. However, it is also likely that the dose to the peritoneal cavity will be a predictor of acute GI complications (5), and Wedlake et al found that cumulative acute GI symptoms, measured using the questionnaire, are associated with consequential late symptoms (14). Collectively, these results suggest that our finding that parameters for the small bowel loops are better predictors of chronic GI complication, compared with those for the peritoneal cavity, requires verification in larger prospective studies.

The findings in this study should be interpreted with an understanding of the following limitations. First, the heterogeneity in the treatment planning approach over the period of the study (2D vs 3D), the low number of events, and the lack of a prespecified model or protocol are important limitations of the data and analysis. Second, our method resulted in large uniform doses to regions of the small bowel, which differ from the dose patterns produced by techniques such as IMRT, which is becoming more prevalent. Therefore, we cannot exclude the possibility that the optimal DVH parameter predictors found in this study may differ from those for IMRT.

Additionally, we used weekly nedaplatin as concurrent chemotherapy, whereas chemoradiation therapy with 40 mg/m^2 of weekly cisplatin is now accepted as a standard first-line treatment. We therefore cannot exclude the possibility that the optimal DVH parameter predictors found in the study may be chemotherapy-type specific. Furthermore, the small bowel DVH parameters were estimated based on only 1 radiation treatment planning CT before RT, while in fact daily variability of the distention or movement of the small bowels during the treatment course may have affected the dose-volume profile. Also, especially in the 2D era, radiation treatment planning CT performed with 5.0-mm slices without filling the bladder may not reflect the actual dose received. Han et al reported that the dose distribution in the small bowel as observed on CT varies significantly from week to week because of the interfractional variations of small-bowel positions (19). In addition, image guided RT is now widely used in many institutions (20). Therefore, further studies using image guided RT will be necessary to investigate the influence of intra- and interfraction motion of the small bowel loops on chronic GI complications.

Within these limitations, we conclude that DVH parameters of the small bowel loops may serve as predictors of chronic GI complications of grade 2 or higher after postoperative concurrent nedaplatin-based chemoradiation therapy in early-stage cervical cancer patients. For these patients, we recommend that V40 of the small bowel loops should be <340 mL to avoid chronic GI complications using a conventional 2D or 3D technique.

References

1. Sedlis A, Bundy BN, Rotman MZ, Lentz SS, Muderspach LI, Zaino RJ. A randomized trial of pelvic radiation therapy versus no further therapy in selected patients with stage IB carcinoma of the cervix after radical hysterectomy and pelvic lymphadenectomy: a Gynecologic Oncology Group Study. *Gynecol Oncol* 1999;73:177-183.
2. Fiorica JV, Roberts WS, Greenberg H, Hoffman MS, LaPolla JP, Cavanagh D, et al. Morbidity and survival patterns in patients after radical hysterectomy and postoperative adjuvant pelvic radiotherapy. *Gynecol Oncol* 1990;36:343-347.
3. Chen SW, Liang JA, Yang SN, Hung YC, Yeh LS, Shiau AC, et al. Radiation injury to intestine following hysterectomy and adjuvant radiotherapy for cervical cancer. *Gynecol Oncol* 2004;95:208-214.
4. Peters WA 3rd, Liu PY, Barrett RJ 2nd, Stock RJ, Monk BJ, Berek JS, et al. Concurrent chemotherapy and pelvic radiation therapy compared with pelvic radiation therapy alone as adjuvant therapy after radical surgery in high-risk early-stage cancer of the cervix. *J Clin Oncol* 2000;18:1606-1613.
5. Kavanagh BD, Pan CC, Dawson LA, Das SK, Li XA, Ten Haken RK, et al. Radiation dose-volume effects in the stomach and small bowel. *Int J Radiat Oncol Biol Phys* 2010;76(Suppl. 3):S101-S107.
6. Mabuchi S, Morishige K, Isohashi F, Yoshioka Y, Takeda T, Yamamoto T, et al. Postoperative concurrent nedaplatin-based chemoradiotherapy improves survival in early-stage cervical cancer patients with adverse risk factors. *Gynecol Oncol* 2009;115:482-487.
7. Mabuchi S, Okazawa M, Isohashi F, Ohta Y, Maruoka S, Yoshioka Y, et al. Postoperative whole pelvic radiotherapy plus concurrent chemotherapy versus extended-field irradiation for early-stage cervical cancer patients with multiple pelvic lymph node metastases. *Gynecol Oncol* 2011;120:94-100.
8. Small W Jr., Mell LK, Anderson P, Creutzberg C, De Los Santos J, Gaffney D, et al. Consensus guidelines for delineation of clinical target volume for intensity-modulated pelvic radiotherapy in postoperative treatment of endometrial and cervical cancer. *Int J Radiat Oncol Biol Phys* 2008;71:428-434.
9. Akobeng AK. Understanding diagnostic tests 3: receiver operating characteristic curves. *Acta Paediatr* 2007;96:644-647.
10. Iraha S, Ogawa K, Moromizato H, Shiraishi M, Nagai Y, Samura H, et al. Radiation enterocolitis requiring surgery in patients with gynecological malignancies. *Int J Radiat Oncol Biol Phys* 2007;68:1088-1093.
11. Kasuya G, Ogawa K, Iraha S, Nagai Y, Shiraishi M, Hirakawa M, et al. Severe late complications in patients with uterine cancer treated with postoperative radiotherapy. *Anticancer Res* 2011;31:3527-3533.
12. Eifel PJ, Jhingran A, Bodurka DC, Levenback C, Thames H. Correlation of smoking history and other patient characteristics with major complications of pelvic radiation therapy for cervical cancer. *J Clin Oncol* 2002;20:3651-3657.
13. Kizer NT, Thaker PH, Gao F, Zighelboim I, Powell MA, Rader JS, et al. The effects of body mass index on complications and survival outcomes in patients with cervical carcinoma undergoing curative chemoradiation therapy. *Cancer* 2011;117:948-956.
14. Wedlake LJ, Thomas K, Lalji A, Blake P, Khoo VS, Tait D, et al. Predicting late effects of pelvic radiotherapy: is there a better approach? *Int J Radiat Oncol Biol Phys* 2010;78:1163-1170.
15. Roeske JC, Lujan A, Rotmensch J, Waggoner SE, Yamada D, Mundt AJ. Intensity-modulated whole pelvic radiation therapy in patients with gynecologic malignancies. *Int J Radiat Oncol Biol Phys* 2000;48:1613-1621.
16. Jhingran A, Winter K, Portelance L, Miller BE, Salehpour M, Gaur R, et al. A phase II study of intensity modulated radiation therapy (IMRT) to the pelvic for post-operative patients with endometrial carcinoma (RTOG 0418). *Int J Radiat Oncol Biol Phys* 2008;72:S16.
17. Mundt AJ, Mell LK, Roeske JC. Preliminary analysis of chronic gastrointestinal toxicity in gynecology patients treated with intensity-modulated whole pelvic radiation therapy. *Int J Radiat Oncol Biol Phys* 2003;56:1354-1360.
18. Chen MF, Tseng CJ, Tseng CC, Kuo YC, Yu CY, Chen WC. Clinical outcome in posthysterectomy cervical cancer patients treated with

concurrent Cisplatin and intensity-modulated pelvic radiotherapy: comparison with conventional radiotherapy. *Int J Radiat Oncol Biol Phys* 2007;67:1438-1444.

19. Han Y, Shin EH, Huh SJ, Lee JE, Park W. Interfractional dose variation during intensity-modulated radiation therapy for cervical cancer assessed by weekly CT evaluation. *Int J Radiat Oncol Biol Phys* 2006; 65:617-623.
20. Simpson DR, Lawson JD, Nath SK, Rose BS, Mundt AJ, Mell LK. A survey of image-guided radiation therapy use in the United States. *Cancer* 2010;116:3953-3960.

Journal of Radiation Research, 2012, 53, 936–944
doi: 10.1093/jrr/rrs035 Advance Access Publication 17 July 2012

The usefulness of an independent patient-specific treatment planning verification method using a benchmark plan in high-dose-rate intracavitary brachytherapy for carcinoma of the uterine cervix

Yutaka TAKAHASHI[1,2,*], Masahiko KOIZUMI[2], Iori SUMIDA[3], Fumiaki ISOHASHI[1], Toshiyuki OGATA[1,2], Yuichi AKINO[1], Yasuo YOSHIOKA[1], Shintaro MARUOKA[1], Shinichi INOUE[4], Koji KONISHI[1] and Kazuhiko OGAWA[1]

[1]Department of Radiation Oncology, Osaka University Graduate School of Medicine, 2-2 Yamada-oka, Suita, Osaka, Japan
[2]Division of Medical Physics, Oncology Center, Osaka University Hospital, 2-15 Yamada-oka, Suita, Osaka, Japan
[3]Department of Radiology, Osaka University Graduate School of Dental Medicine, 1-8 Yamada-oka, Suita, Osaka, Japan
[4]Department of Medical Technology, Osaka University Hospital, 2-15 Yamada-oka, Suita, Osaka, Japan
*Corresponding author. Tel: 81-6-6879-3482; Email: ytakahashi@radonc.med.osaka-u.ac.jp

(Received 2 March 2012; revised 15 May 2012; accepted 18 May 2012)

To develop an easy independent patient-specific quality assurance (QA) method using a benchmark plan for high-dose-rate intracavitary brachytherapy for cervix cancer, we conducted benchmark treatment planning with various sizes and combinations of tandem-ovoid and tandem-cylinder applications with 'ideal' geometry outside the patient. Two-dimensional-based treatment planning was conducted based on the Manchester method. We predicted the total dwell time of individual treatment plans from the air kerma strength, total dwell time and prescription dose of the benchmark plan. In addition, we recorded the height (dh), width (dw) and thickness (dt) covered with 100% isodose line. These parameters were compared with 169 and 29 clinical cases for tandem-ovoid or tandem-cylinder cases, respectively. With regard to tandem-ovoid cases, differences in total dwell time, dh, dt and dw between benchmark and individual plans were on average $-0.2\% \pm 3.8\%$, -1.0 mm $\pm$ 2.6 mm, 0.8 mm $\pm$ 1.3 mm and -0.1 mm $\pm$ 1.5 mm, respectively. With regard to tandem-cylinder cases, differences in total dwell time, dh_{front} (the distance from tandem tip to tandem ring), dt and dw between benchmark and individual plans were on average $-1.5\% \pm 3.1\%$, -1.5 mm $\pm$ 4.9 mm, 0.1 mm $\pm$ 1.0 mm and 0.2 mm $\pm$ 0.8 mm, respectively. Of two cases, more than 13% differences in total dwell time were observed between benchmark plans and the clinical cases, which turned out to be due to the use of the wrong source position setting. These results suggest that our method is easy and useful for independent verification of patient-specific treatment planning QA.

Keywords: independent verification; treatment planning; Manchester method; benchmark plan; high-dose-rate intracavitary brachytherapy; uterine cervix

INTRODUCTION

Brachytherapy is an essential component of radiotherapy for the carcinoma of uterine cervix and is often combined with external beam radiation therapy (EBRT) for radical treatment. Several studies have suggested that control rates are significantly improved with EBRT and brachytherapy [1, 2]. High-dose-rate (HDR) remote afterloading intracavitary brachytherapy is widely used throughout Asia and Europe [3], and is becoming steadily more common in the USA [4].

The importance of independent verification of dosimetry prior to HDR brachytherapy treatment delivery has been recognized worldwide, and is specified in the guidelines of international regulatory agencies [5]. The Nuclear Regulation Commission (NRC) considers a 20% difference between the prescribed total dose and delivered dose to be a reportable medical event [5]. Thomadsen *et al.* identified 44 medical events in HDR brachytherapy between 1980 and 2001 in data from the NRC and International Atomic Energy Agency [6]. In fact, patients are often required to

© The Author 2012. Published by Oxford University Press on behalf of The Japan Radiation Research Society and Japanese Society for Therapeutic Radiology and Oncology.
This is an Open Access article distributed under the terms of the Creative Commons Attribution Non-Commercial License (http://creativecommons.org/licenses/by-nc/3.0/), which permits unrestricted non-commercial use, distribution, and reproduction in any medium, provided the original work is properly cited.

wait during treatment planning with an applicator inserted by a radiation oncologist, during which time errors and miscommunications can easily occur. This situation clearly indicates that patient-specific quality assurance (QA), including independent verification of treatment planning and confirmation of applicator geometry, should be done quickly and easily.

Many studies have reported independent verification methods for HDR brachytherapy treatment planning [7–16]. More recent reports have focused on the development of in-house software based on the AAPM TG 43 [17] formulism to calculate the dose at arbitrary points [13–15]. Although such software might be useful for the commissioning of treatment planning systems, human errors in individual treatment planning in clinical practice will not be identified due to the use of the same coordinate system, digitized applicator paths and dose point coordinates as those in the treatment planning system.

Although image-guided intracavitary brachytherapy has been enthusiastically investigated [18], treatment planning based on the Manchester method using two projection radiographs is still used [3]. One of the goals in intracavitary brachytherapy for carcinoma of the uterine cervix is to achieve the same level of consistency as the Manchester method. We have established the Osaka University Protocol based on the Manchester method with some modifications [19]. The goal of our institution is to achieve consistency with our protocol-based benchmark plans.

Here, we propose a very quick, simple and easy patient-specific independent verification method for Manchester method-based treatment planning using benchmark plans to detect human errors and evaluate the quality of the applicator geometry in the patient.

MATERIALS AND METHODS

Creation of benchmark plans

In this study, Fletcher-type (Fletcher-Williamson Asian-Pacific) tandem-ovoid and tandem-cylinder metal applicators (Nucletron International B.V., Veendaal, the Netherlands) were used. Various sizes and combinations of these applicators were constructed by one radiation oncologist with the 'ideal' applicator geometry outside the patient (Fig. 1a and b) and then reviewed by a medical physicist. We constructed eight kinds of tandem-ovoid and six kinds of benchmark plans (Table 1).

Figure 1c shows the 'ideal' geometry of a tandem-ovoid applicator used in our institution. Namely, a flange on the tandem tube is used at the origin, which is the cervical os

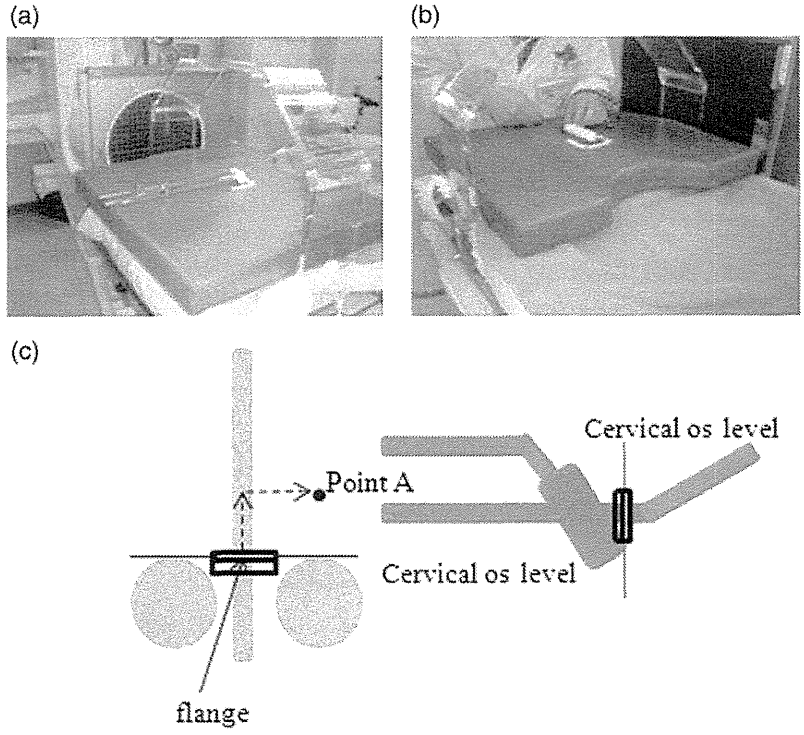

Fig. 1. Creation of benchmark plans. (**a**) Scheme for the construction of tandem-ovoid; (**b**) tandem-cylinder applications; (**c**) typical dose distribution with the tandem-ovoid application.

Table 1. Applicator settings used in benchmark plans

Tandem-ovoid			Tandem-cylinder		
Tandem length (cm)	Ovoid size		Cylinder diameter (cm)		
4	S	SS	2	2.5	3
5	S	SS	N/A	N/A	N/A
6	S	SS	2	2.5	3
7	S	SS	NA	NA	NA

The ovoid diameter of S size is 2.0 cm. The size of SS ovoid is half-cut-size of S ovoid. NA, not applicable.

and the tip of the ovoid is aligned with the origin (a flange on the tandem). Using these ideal applicator settings, treatment planning was performed with PLATO (Nucletron International B.V). Source dwell time was manually optimized based on the Manchester method as demonstrated by Tod and Meredith with minor modification [19–21]. Air kerma strength and total dwell time were then recorded. All benchmark plans were constructed by a medical physicist and reviewed by another medical physicist.

Prediction of total dwell time for individual patient treatments

Dose was calculated with the following formula introduced in AAPM TG43-U1 [22].

$$D(r,\theta) = S_K \times \Lambda \times \frac{G_L(r,\theta)}{G_L(r_0,\theta_0)} \times g_L(r) \times F(r,\theta) \times \text{dwell time} = S_k \times \text{dwell time} \times A$$

where S_K, Λ, G_L, g_L and F represent air kerma strength, dose rate constant, geometric function, radial dose function and anisotropy function, respectively. Here, we defined A as the product of Λ, G_L, $g_L(r)$ and $F(r, \theta)$.

The dose at the reference point in the benchmark plan is therefore calculated by the following:

$$D(r,\theta)_b = A_b \times S_{K\_b} \times \text{dwell time}_b \quad (1)$$

Similarly, the dose at point A in the individual plan is calculated by the following:

$$D(r,\theta)_t = A_b \times S_{K\_t} \times \text{dwell time}_t \quad (2)$$

If the 'ideal' tandem-ovoid geometry is achieved in the patient without any planning errors or misuse of the applicator, A_b is nearly equal to A_t. Dwell time in the individual plan can therefore be predicted by the following formula from (1) and (2):

$$\text{Dwell time}_t = \frac{D(r,\theta)_t \times S_{K\_b} \times \text{dwell time}_b}{D(r,\theta)_b \times S_{K\_t}} \quad (3)$$

where $D(r, \theta)_t$ and $D(r, \theta)_b$ represent the prescription dose of each treatment and the benchmark plan, respectively.

Comparison of dose shape with that of the benchmark plans

ICRU report 38 [23] recommends reporting the reference volume as well as total reference air kerma strength and absorbed dose at reference points. The reference volume is the volume encompassed by the reference isodose surface, which is represented by the major dimensions of the following:

(i) Height (dh), which is the maximum dimension along the tandem source measured on an 'oblique' sagittal plane;
(ii) Thickness (dt), which is the maximum dimension perpendicular to the tandem sources measured on a transverse plane;
(iii) Width (dw), which is the maximum dimension perpendicular to the tandem sources measured on a transverse plane.

In addition to the above parameters, we defined the dimensions of dh_{front} and dh_{ext}, which represent the distance from th 100% isodose line of the tip side of the tandem to the origin and that from the 100% isodose line of the connector side of the tandem to the origin, respectively (Fig. 2c).

Figure 2 shows the definitions of these parameters. For the tandem-cylinder, we recorded the additional parameters of dh_{front} and dh_{ext}, which represent the maximum dimension of the 100% isodose line of the tip side of the tandem to the tandem flange, and that of the connector side of the tandem to the tandem flange (Fig. 2c). These values were measured for individual treatment plans and compared with those of the benchmark plans.

Analysis of clinical cases

We retrospectively analyzed 168 and 29 clinical cases from 2009 through 2010 with a tandem-ovoid and tandem-cylinder, respectively. The difference in total dwell time between a benchmark plan and an individual treatment plan was calculated using the following formula:

$$\text{Relativedifference}(\%) = \frac{T_{\text{individual}} - T_{\text{benchmark}}}{T_{\text{benchmark}}} \times 100$$

where $T_{benchmark}$ and $T_{individual}$ represent the total dwell time of the benchmark and individual plans, respectively. Differences in dose distribution shapes, including dh or dh_{front}, and dh_{ext}, dt, and dw between the benchmark and

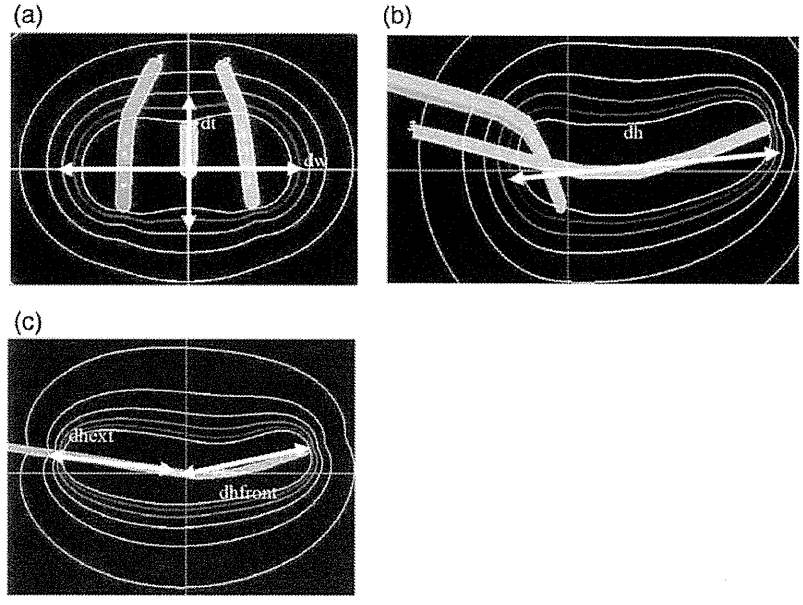

Fig. 2. Definitions of dh, dhfront, dhext, dt and dw used in this study based on ICRU report 38 [23]. These parameters were defined in the plane of the cervical os. (**a**) Transverse plane of tandem-ovoid case; (**b**) sagittal plane of tandem-ovoid case; (**c**) sagittal plane of tandem-cylinder case. Red line shows the isodose line of 100% of the prescription dose.

individual plans were calculated using the following formula:

$$\text{Relativedifference} = \text{shape}_{\text{benchmark}} - \text{shape}_{\text{individual}}$$

Where $\text{shape}_{\text{benchmark}}$ and $\text{shape}_{\text{individual}}$ represent the dose distribution shapes of the benchmark and individual treatment plans, respectively.

Correlations between the differences in total dwell time and those in dh, dt or dw among the benchmark and individual treatment plans were evaluated by Spearman's rank correlation coefficient using Dr. SPSS II software (IMB, New York, USA).

Tolerance levels for total dwell time, dh or dh_{front}, and dh_{ext}, dt, and dw were calculated by the following formula, which was first proposed by Venselaar *et al.* [24]

Tolerance level = mean deviation ± 1.96 SD

RESULTS

Tandem-ovoid cases

Prediction of total dwell time for individual treatment plans

Figure 3 shows a histogram of differences in total dwell time between benchmark and individual treatment plans.

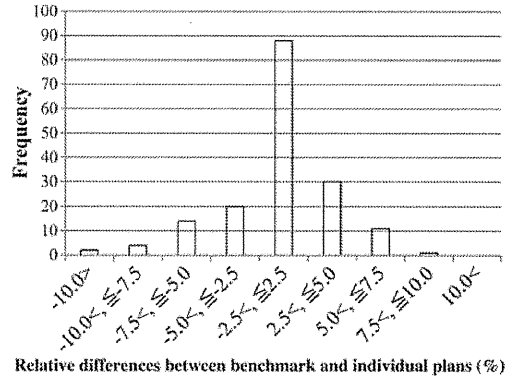

Fig. 3. Histogram of % differences in total dwell time between the benchmark and individual treatment plans.

Differences averaged –0.2% ± 3.8% (range, –13.3–9.6%), and exceeded 5% in 23 of 169 clinical cases.

Comparison of the dose distribution shapes of individual treatment plans with those of the benchmark plans

Figure 4 shows a histogram of differences in dose distribution shapes between the benchmark and individual treatment plans in tandem-ovoid applications. The differences in

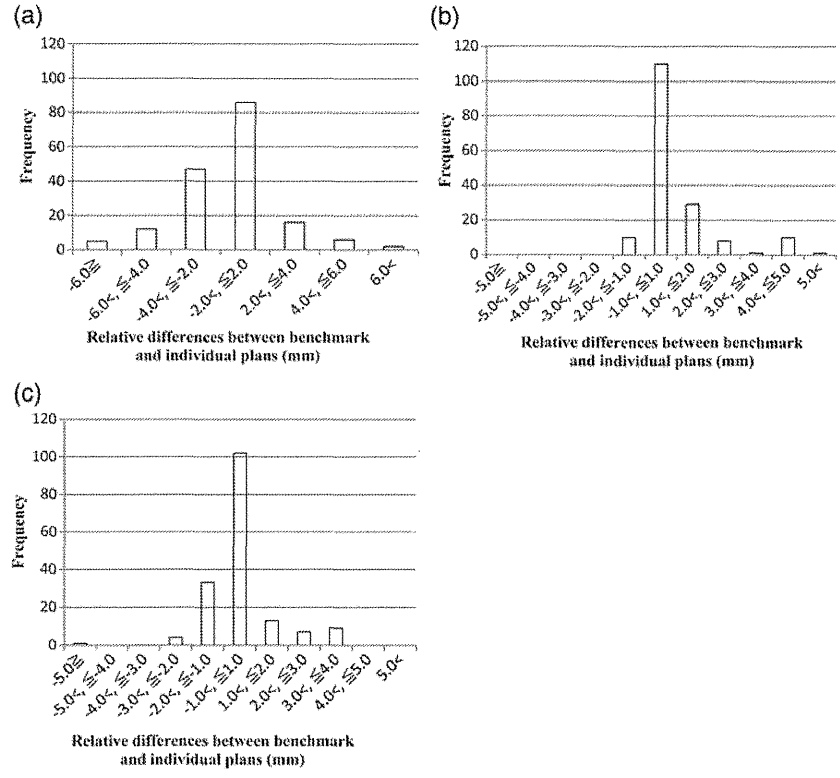

Fig. 4. Histogram of differences in (**a**) dh, (**b**) dt and (**c**) dw between the benchmark and individual treatment plans in mm.

dh, dt and dw between the benchmark and individual plans averaged –1.0 mm ± 2.6 mm (range, –8.6 mm to +6.5 mm), 0.8 mm ± 1.3 mm (range, –1.4 mm to +5.2 mm) and –0.1 mm ± 1.5 mm (range, –5.1 mm to +4.0 mm), respectively.

Regarding dh, 9 of 169 cases showed a difference between the benchmark and individual plans of greater than 5 mm. For dt and dw, in contrast, only one case showed a difference of more than 5 mm.

Subset analysis of cases with large deviations between the benchmark and individual treatment plans

We verified that all tandem-ovoid treatment plans were appropriately created without any planning errors, including wrong source position, wrong decay correction of source strength and inappropriate optimization or use of an unplanned size or combination of applicators. However, 24 of 169 cases had a >5% difference in total dwell time. To explain these differences, we investigated the correlation between differences in total dwell times and dh, dt and dw between the benchmark and individual plans. Figure 5a shows the relationship of differences in total dwell time (vertical axis) with those in dh (horizontal axis). Spearman's rank correlation coefficient ($r_s = 0.836$, $P < 0.01$) showed a strong relationship between the discrepancy in total dwell time and those in dh. In contrast, no correlations were found between the discrepancy in total dwell time and those in dt ($r_s = 0.371$, $P = 0.075$) or dw ($r_s = 0.290$, $P = 0.149$) (Fig. 5b and c).

Tandem-cylinder cases

Figure 6a shows differences in total dwell time between the benchmark and individual treatment plans. Differences averaged –1.5% ± 3.1% (range, –13.0% to +0.4%), with 2 of 29 cases exceeding 11%.

Figure 6b shows the differences in dh_{front}, dh_{ext}, dt and dw between the benchmark and individual treatment plans. Differences averaged –1.5 mm ± 4.9 mm (range, –19.0 mm to +4.0 mm), +1.8 mm ± 5.2 mm (range, –2.2 mm to +20.8 mm), +0.1 mm ± 1.0 mm (range, –1.3 mm to +4.3 mm) and +0.2 mm ± 0.8 mm (range, –0.4 mm to +3.9 mm), respectively. The differences in 2 of 29 cases, which also exceeded an 11% difference in total dwell time, exceeded –19 mm and +20 mm for dh_{front} and dh_{ext}, respectively. These cases were found to have been treated

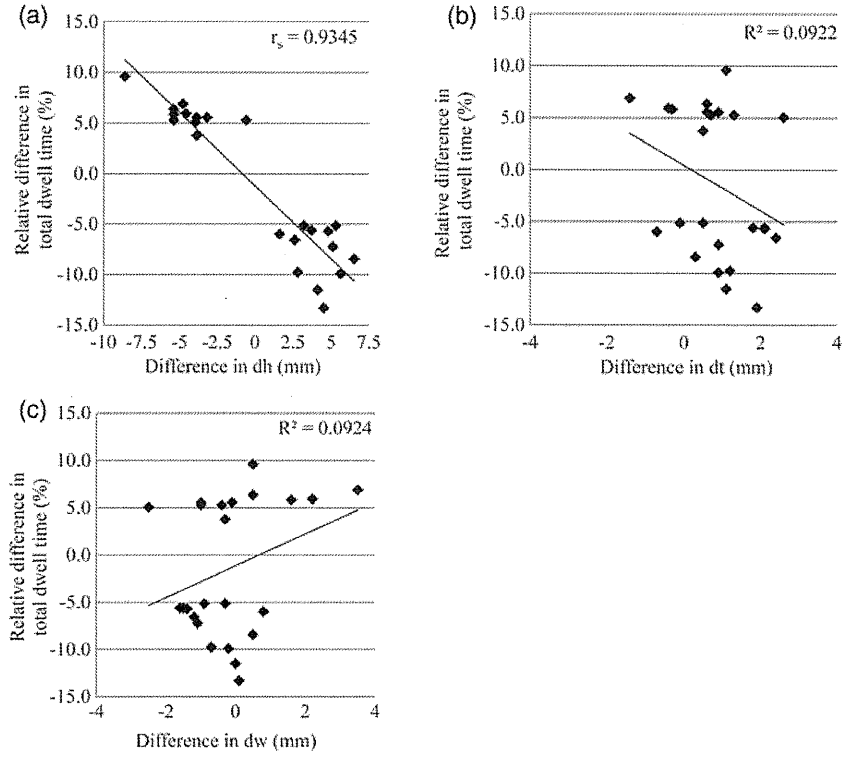

Fig. 5. Correlations between the differences in total dwell time and in (**a**) dh, (**b**) dt and (**c**) dw. Vertical axis shows the % differences in total dwell time between the benchmark and individual treatment plans, and the horizontal axis shows the differences in dh, dt or dw in mm between the benchmark and individual treatment plans.

with an unplanned tandem length, resulting in an incorrect setting for the source dwell positions in treatment planning.

Determination of tolerance limit

For tandem-ovoid cases, the tolerance level of total dwell time, dh, dt, and dw were –7.5% to +7.2, –6.0 mm to +4.1 mm, –1.8 mm to +3.4 mm and –3.0 mm to +2.8 mm, respectively (Fig. 7a).

For tandem-cylinder cases, two cases were excluded from the determination of tolerance limits because they were human error-related. Tolerance limits for total dwell time, dh_{front}, dh_{ext}, dt, and dw were –2.5% to +1.1%, –2.6 mm to +2.3 mm, –2.2 mm to +3.0 mm, –0.9 mm to +0.6 mm and –0.4 mm to +0.4 mm, respectively (Fig. 7b).

DISCUSSION

We used benchmark plans to establish a highly simple, easy, and fast independent treatment planning verification method for high-dose-rate intracavitary brachytherapy for carcinoma of the uterine cervix that requires no special skills such as developing TG43-based in-house software. Despite its great simplicity, analysis of a large number of clinical cases showed that our method was able to detect human error-related planning mistakes, and to evaluate the quality and consistency of applicator geometry.

The Manchester method, which was first suggested by Tod and Meredith in 1938, has been the most broadly used for the treatment of carcinomas of the uterine cervix, with some modifications from the original [20, 21]. They demonstrated an 'ideal' system in which loading patterns of milligrams of radium were determined based on the size of the tandem and ovoids to achieve as constant a dose rate at point A as possible, no matter what combination of applicators was used, and to ensure a suitable ratio between the intra-uterine and vaginal contribution [21]. This rule has been applied to high-dose-rate brachytherapy with an Ir-192 stepping source by modulating the weight of dwell times. In our institution, manual optimization in treatment planning is also based on the Manchester method with some modifications [19]. In addition, the applicator is set such that its geometry is consistent with the 'ideal' geometry specified in the benchmark plan. If there were any planning errors and inappropriate applicator setting, total

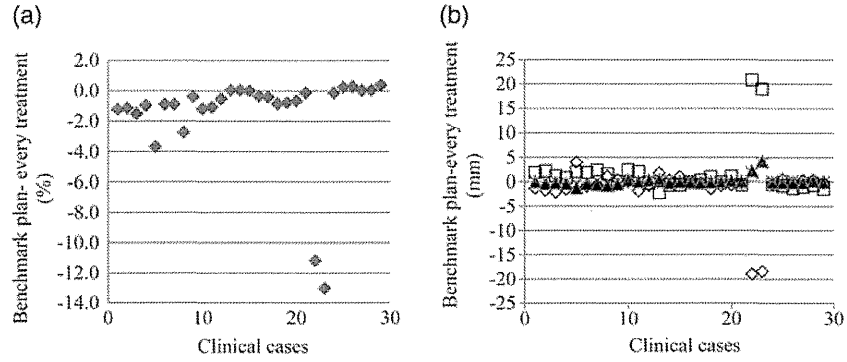

Fig. 6. Differences in (**a**) total dwell time, and (**b**) dh_{front}, dh_{ext}, dt and dw between the benchmark plans and clinical cases in tandem-cylinder settings. White squares, dh_{ext}; white diamonds, dh_{front}; black triangles, dt; and crosses, dw.

dwell time and dose distribution shapes, including dh, dt and dw, in individual treatment plans should agree with those of the benchmark plan. From these points, we established a method for the independent verification of patient-specific treatment planning QA by comparing benchmark plans with individual treatment plans.

Several other independent verification methods for individual treatment planning have been reported. Kumar *et al.* developed an in-house application that calculates the dose at arbitral points [13]. Lachaine *et al.* also developed an in-house application that achieves very fast calculation of point dose [14]. Such kind of applications are likely to be useful in the commissioning of treatment planning systems and partly also in individual treatment planning QA in terms of parameters such as source strength, treatment date and source table, which users input by themselves. However, because these applications use the same Cartesian coordinate system, digitized applicator paths and dose point coordinates as those in the treatment planning system, they are unable to detect human errors associated with the treatment planning process, such as setting of prescription point (Point A) with the wrong coordinate, the incorrect digitization of applicators, incorrect dose points or applicator points, improper magnification of simulation films, or use of an unplanned size or combination of applicators.

Several groups have previously proposed a method of checking total dwell time as a fraction of treatment length and dose prescription, or dose area index for planar implants and single catheter interstitial brachytherapy [8–11]. Recently, for example, Das *et al.* reported that total dwell time can be predicted from the reference volume covered with the prescribed dose (V100) in both single catheter and multiple catheter interstitial implants by the retrospective analysis of V100 from many clinical cases [12]. All these reports were focused on interstitial implants rather than intracavitary brachytherapy, however, and little information on intracavitary brachytherapy for carcinoma of the uterine cervix is available. In 1992, Thomadsen *et al.* demonstrated a method that assures the consistency of dwell times and dose distribution with previous treatment fractions and

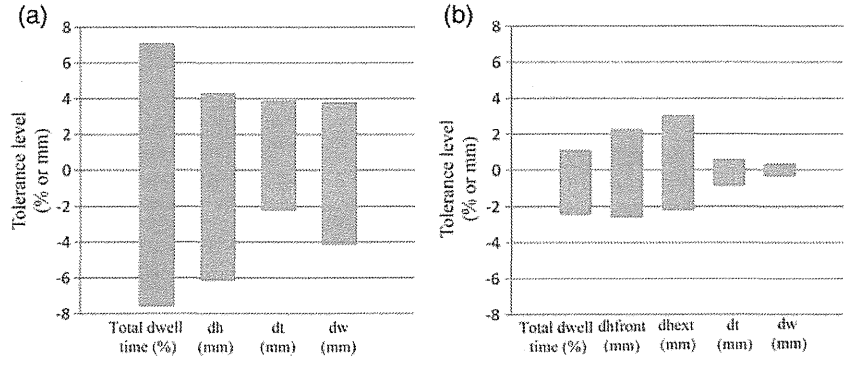

Fig. 7. Tolerance levels of (**a**) tandem-ovoid and (**b**) tandem-cylinder.

previous patients [7]. Although our method is basically similar to their concepts, we created benchmark plans in which the 'ideal' geometry of the tandem-ovoid or tandem-cylinder can be achieved because these applications are constructed outside the patient's body. Therefore the geometry of the applicator can be evaluated in every treatment by comparison with that of the 'ideal' geometry in the benchmark plan.

Although many independent verification methods have been reported, as described above, our present study is one of only a few to evaluate the usefulness of the method in a large number of clinical cases of intracavitary brachytherapy. In tandem-cylinder cases, two cases were found to have >11% differences in total dwell time between the benchmark and individual treatment plans, and >18 mm differences in dh_{front} and dh_{ext}. Review of these two cases showed that these differences were due to the unplanned use of tandem length, which resulted in the use of incorrect settings for the source dwell positions in treatment planning. The results clearly demonstrate that our method can easily identify such kinds of human error.

Regarding tandem-ovoid cases, a thorough review revealed no human-related planning errors. We next examined the reason why 24 cases of tandem-ovoid cases had >5% differences in total dwell time between the benchmark and individual plans. We found that these differences strongly correlated with differences in dh (Fig. 6), indicating that when the ovoid position shifts cranially compared with the benchmark plan, total dwell time decreases because the distance between the sources in the ovoids and point A becomes shorter. Conversely, if the ovoid position shifts caudally to the tandem flange compared with the benchmark plan, total dwell time increases, because the distance between sources in the ovoids and point A becomes larger. These facts indicate that our method is useful in not only finding human errors and software bugs but also in evaluating the quality of the applicator insertion technique. In other words, the evaluation of both the differences in total dwell time and dh could provide a good indicator for the quality of the applicator's geometry.

We set tolerance limits for differences in total dwell time and dose shape between the benchmark and individual treatment plans. Ezell *et al.* reported that they set action levels for per-patient intensity modulated radiation therapy verification using confidence limits [25], as first proposed by Venselaar *et al.* [24]. If the confidence limit is established with sufficient points to provide good statistics, then the value of 1.96σ suggests that variations in excesses of the limit would occur about 5% of the time. We determined the tolerance limits by using confidence limits for total dwell time, dt, dh (dh_{front}, and dh_{ext} for tandem-cylinder cases) and dw. To calculate tolerance limits, we excluded the two cases with >18% differences in tandem-cylinder cases to eliminate the effect of human error-related planning mistakes. These tolerance limits might be one indicator in the evaluation of individual treatment plans (i.e. rechecking of treatment planning, use of appropriate size of applicators, inappropriate applicator geometry, etc.).

One limitation of our study warrants mention, namely that our method is useful only for Manchester-based intracavitary brachytherapy. For carcinoma of the uterus, however, most treatment centers in the world have followed a traditional concept based on the Manchester loading patterns [3, 26]. Moreover, local control rates are significantly improved with EBRT and brachytherapy based on the Manchester method [1]. Our method therefore appears useful despite this limitation.

In conclusion, we established a highly simple, easy and quick independent verification method using benchmark plans for intracavitary brachytherapy based on the 2D-based Manchester method. Despite the great simplicity, our method can evaluate the quality of the applicator insertion technique, as well as identify human errors in treatment planning.

ACKNOWLEDGEMENTS

This study was supported by Grants-in-Aid for Scientific Research (22791194) from the Japan Society for the Promotion of Science. This study was also supported by the Japanese Society of Therapeutic Radiology and Oncology and Grants-in-Aid for Cancer Research (Nos. 23-3-3rd Term Cancer Control-General-007) from the Ministry of Health, Labor and Welfare of Japan.

REFERENCES

1. Lanciano RM, Martz K, Coia LR *et al.* Tumor and treatment factors improving outcome in stage III-B cervix cancer. *Int J Radiat Oncol Biol Phys* 1991;**20**:95–100.
2. Montana GS, Fowler WC, Varia MA *et al.* Carcinoma of the cervix, stage III. Results of radiation therapy. *Cancer* 1986;**57**:148–54.
3. Toita T. Current status and perspectives of brachytherapy for cervical cancer. *Int J Clin Oncol* 2009;**14**:25–30.
4. Nag S, Orton C, Young D *et al.* The American brachytherapy society survey of brachytherapy practice for carcinoma of the uterine cervix in the United States. *Gynecol Oncol* 1999;**73**:111–8.
5. NRC. US Nuclear Regulatory Commission. Title 10, Chapter 1, *Code of Federal Regulations d Energy. Part 35. Medical Use of By-product Material.* Washington, DC: Government Printing office, 2003.
6. Thomadosen BR, Lin SW, Laemmrich P *et al.* Analysis of treatment delivery error in brachytherapy using formal risk analysis techniques. *Int J Radiat Oncol Biol Phys* 2003; **57** (5):1492–508.
7. Thomadosen BR, Shahabi S, Stitt JA *et al.* High dose rate intracavitary brachytherapy for carcinoma of the cervix: The

Madison system: II. Procedural and physical considerations. *Int J Radiat Oncol Biol Phys* 1992;**24**:349–57.
8. Venselaar JLM, Bierhuizen HWJ, Klop R. A method to check treatment time calculations in Ir-192 high dose rate volume implants. *Med Phys* 1996;**22**:1499–500.
9. Ezzell GA. Quality assurance of treatment plans for optimized high dose rate brachytherapy planar implants. *Med Phys* 1994;**21**:659–61.
10. Rogus RD, Smith MJ Kubo HD. An equation to QA check the total treatment time for single-catheter HDR brachytherapy. *Int J Radiat Oncol Biol Phys* 1998;**40**:245–8.
11. Kubo HD. Verification of treatment plans by mathematical formulas for single catheter HDR brachytherapy. *Med Dosim* 1992;**17**:151–5.
12. Das RK, Bradley KA, Nelson IA *et al.* Quality assurance of treatment plans for interstitial and intracavitary high-dose-rate brachytherapy. *Brachytherapy* 2006;**5**:56–60.
13. Kumar R, Sharma SD, Vijaykumar C *et al.* A dose verification method for high-dose-rate brachytherapy treatment plans. *J Cancer Res Ther* 2008;**4**(4):173–7.
14. Lachaine ME, Gorman JC, Palisca MG. A fast independent dose check of HDR plans. *J Appl Clin Med Phys* 2003;**4**(2):149–55.
15. Cohen GN, Amols HI, Zaider M. An independent dose-to-point calculation program for the verification of high-dose-rate brachytherapy treatment planning. *Int J Radiat Oncol Biol Phys* 2000;**48**(4):1251–8.
16. Bidmead M, Briot E, Burger J *et al.* Quality assurance of brachytherapy treatment planning system. In: Venselaar J, Calatayud JP (eds) *A Practical Guide to Quality Control of Brachytherapy Equipment*. Brussels: ESTRO, 2004, 215–31.
17. Nath R, Anderson L, Luxton G *et al.* Dosimetry of interstitial brachytherapy sources: recommendations of the AAPM Radiation Therapy Committee Task Group No. 43. *Med Phys* 1995;**22**:209–34.
18. Toita T, Kodaira T, Shinoda A *et al.* Patterns of radiotherapy practice for patients with cervical cancer (1999–2001): patterns of care study in Japan. *Int J Radiat Oncol Biol Phys* 2008;**70**:788–94.
19. Teshima T, Inoue T, Ikeda H *et al.* High-dose-rate versus low-dose-rate intracavitary therapy for carcinoma of the uterine cervix. Final results of Osaka University Hospital. *Cancer* 1993;**72**:2409–14.
20. Tod M, Merdith W. Treatment of cancer of the cervix uteri, a revised Manchester method. *Br J Radiol* 1953;**26**:252–7.
21. Tod M, Merdith W. A dosage system for use in the treatment of cancer of the uterine cervix. *Br J Radiol* 1938;**11**:809–24.
22. Rivard M, Coursey B, DeWerd L *et al.* Update of AAPM Task Group No.43 Report: a revised AAPM protocol for brachytherapy dose calculations. *Med Phys* 2004;**31**:633–74.
23. ICRU, International Commission on Radiation Units, Measurements. Dose and Volume Specification for Reporting Intracavitary Therapy in Gynecology, *ICRU Report No. 38*. Bethesda, MD: ICRU, 1985.
24. Venselaar J, Welleweerd H, Mijnheer B. Tolerances for the accuracy of photon beam dose calculation of treatment planning system. *Radiother Oncol* 2001;**60**:191–201.
25. Ezzel GA, Burmeister JW, Dogan N. IMRT commissioning: multiple institution planning dosimetry comparisons a report from AAPM task group 119. *Med Phys* 2009;**36**(11):5359–73.
26. Jamema SVJ, Kirisits C, Mahantshetty U *et al.* Comparison of DVH parameters and loading patterns of standard loading, manual and inverse optimization for intracavitary brachytherapy on a subset of tandem/ovoid cases. *Radiother Oncol* 2010;**97**:501–6.

Int. J. Radiation Oncology Biol. Phys., Vol. 82, No. 5, pp. 1715–1722, 2012
Copyright © 2012 Elsevier Inc.
Printed in the USA. All rights reserved
0360-3016/$ - see front matter

ELSEVIER

doi:10.1016/j.ijrobp.2011.03.034

PHYSICS CONTRIBUTION

MEGAVOLTAGE CONE BEAM COMPUTED TOMOGRAPHY DOSE AND THE NECESSITY OF REOPTIMIZATION FOR IMAGING DOSE-INTEGRATED INTENSITY-MODULATED RADIOTHERAPY FOR PROSTATE CANCER

YUICHI AKINO, M.S.,* MASAHIKO KOIZUMI, M.D.,† IORI SUMIDA, PH.D.,*† YUTAKA TAKAHASHI, PH.D.,*† TOSHIYUKI OGATA, M.S.,*† SEIICHI OTA, B.S.,‡ FUMIAKI ISOHASHI, M.D.,* KOJI KONISHI, M.D.,* AND YASUO YOSHIOKA, M.D.*

*Department of Radiation Oncology, Osaka University Graduate School of Medicine, Suita, Osaka, Japan; †Division of Medical Physics, Oncology Center, and ‡Division of Radiology, Department of Medical Technology, Osaka University Hospital, Suita, Osaka, Japan

Purpose: Megavoltage cone beam computed tomography (MV-CBCT) dose can be integrated with the patient's prescription. Here, we investigated the effects of imaging dose and the necessity for additional optimization when using intensity-modulated radiotherapy (IMRT) to treat prostate cancer.

Methods and Materials: An arc beam mimicking MV-CBCT was generated using XiO (version 4.50; Elekta, Stockholm, Sweden). The monitor units (MU) for dose calculation were determined by conforming the calculated dose to the dose measured using an ionization chamber. IMRT treatment plans of 22 patients with prostate cancer were retrospectively analyzed. Arc beams of 3, 5, 8, and 15 MU were added to the IMRT plans, and the dose covering 95% of the planning target volume (PTV) was normalized to the prescribed dose with (reoptimization) or without optimization (compensation).

Results: PTV homogeneity and conformality changed negligibly with MV-CBCT integration. For critical organs, an imaging dose-dependent increase was observed for the mean rectal/bladder dose (D_{mean}), and reoptimization effectively suppressed the D_{mean} elevations. The bladder generalized equivalent uniform dose (gEUD) increased with imaging dose, and reoptimization suppressed the gEUD elevation when 5- to 15-MU CBCT were added, although rectal gEUD changed negligibly with any imaging dose. Whereas the dose elevation from the simple addition of the imaging dose uniformly increased rectal and bladder dose, the rectal D_{mean} increase of compensation plans was due mainly to low-dose volumes. In contrast, bladder high-dose volumes were increased by integrating the CBCT dose, and reoptimization reduced them when 5- to 15-MU CBCT were added.

Conclusion: Reoptimization is clearly beneficial for reducing dose to critical organs, elevated by addition of high-MU CBCT, especially for the bladder. For low-MU CBCT aimed at bony structure visualization, compensation is sufficient. © 2012 Elsevier Inc.

Dose compensation, Megavolt cone beam computed tomography, Prostate IMRT, Reoptimization.

INTRODUCTION

Megavoltage cone beam computed tomography (MV-CBCT) using a MV treatment beam and an electronic portal imaging device enables precise quantitative evaluation of patient setup error (1–3). The technology allows verification of organ alignment and estimation of the actual dose delivered to patients (4–6). Advantages of MV-CBCT include its stable geometry and low incidence of metal artifacts compared to kilovoltage CBCT (kV-CBCT). Disadvantages include elevated dose (7) and low image contrast compared to kV-CBCT (8), although improvements to the latter have been made (9, 10).

Intensity-modulated radiotherapy (IMRT) allows a reduction in the dose to organs at risk (OARs) by modulating the beam intensity in each beam field, using a multileaf collimator (11, 12). Pelvic organs exhibit both systematic and random motions, deformations, and size variations during treatment and over the entire course of therapy (13–16). Achieving the desired dose distribution requires still more accurate patient setup, as any uncertainty will be

Reprint requests to: Masahiko Koizumi, M.D., Ph.D., Division of Medical Physics, Oncology Center, Osaka University Hospital, 2-2(D10), Yamadaoka, Suita, Osaka, 565-0871, Japan. Tel: (+81) 6 6879 3482; Fax: (+81) 6 6879 3489; E-mail: koizumi@radonc.med.osaka-u.ac.jp

Conflict of interest: none.

Acknowledgment—This work was supervised by the late Takehiro Inoue, Professor, Department of Radiation Oncology, Osaka University Graduate School of Medicine. We gratefully thank him for his wise counsel regarding the design, analysis, and reporting of this study.

Received May 11, 2010, and in revised form Feb 10, 2011. Accepted for publication March 22, 2011.

accompanied by deformation of dose distribution, resulting in the failure of dose delivery to targets and elevated dose to OARs (17). For setup verification in our institution, we routinely used a monitor unit (MU) value of 3 for CBCT, which is the minimum value for image acquisition protocols. We verified that the image quality of 3-MU CBCT was adequate for recognizing skeletal structures. For soft tissue visualization, however, we consider that 8 or more MU are required, based on clinical experience. Similarly, Morin et al. (1, 18) have suggested that the image contrast of 9-MU CBCT is sufficient for soft tissue visualization. Typically, an IMRT series consists of many fractions, and the contribution of the MV-CBCT dose may be unacceptable if image acquisition with high MU is applied to every treatment fraction. The characteristics of the CBCT beam are quite similar to those of the treatment beam, meaning that MV-CBCT dose distribution can be estimated using a radiotherapy treatment planning system (RTPS) (2). Morin et al. (18) introduced a methodology for integrating MV-CBCT dose with the prescribed dose, which used 5 MU for the head and neck region and 9 MU for the pelvic region. Those imaging doses were integrated into prescribed doses for radiotherapy by scaling down the dose weights from the total prescribed dose of the treatment beams. Miften et al. (19) showed that IMRT optimization performed after addition of the MV-CBCT beam reduced OAR dose by taking into consideration the contribution of the MV-CBCT beam. That study's MV-CBCT protocols used 15 MU for the pelvic region. The MU values for MV-CBCT were fixed in those studies, and no study has investigated the effects of MU alteration on dose distribution, although imaging dose is known to affect both patient dose and MV-CBCT image quality (2, 20).

Here, we investigated the effects of MV-CBCT imaging dose alteration and the necessity for reoptimizing MV-CBCT dose-integrated IMRT related to dose distribution in treating prostate cancer.

METHODS AND MATERIALS

Linear accelerator and MV-CBCT system

Our institution's Oncor Impression Plus linear accelerator (LINAC) with Optifocus multileaf collimator (both from Siemens Medical Solutions, Concord, CA) is capable of generating dual-energy X-ray beams (6 and 10 MV). An MVision MV-CBCT system (Siemens Medical Solutions) was installed. During MV-CBCT acquisition, the gantry of the LINAC rotates from 270° to 110°, generating a 6-MV photon beam. The field width of the MV-CBCT system is 27.4 cm. The maximum range in the superior-inferior direction is 27.4 cm, and the range can be adjusted using Y-jaws.

Dose calculation and verification of MV-CBCT accuracy

Dose distribution for MV-CBCT and treatment planning was done using an XiO version 4.50 (Elekta, Stockholm, Sweden) treatment planning system. The MV-CBCT system with doses of 3, 5, 8, and 15 MU (set MU) was calculated by regarding it as an arc beam with a gantry rotation from 270° to 110°. The calculation step of the arc beam was 10°. Field length along the Y-axis (superior-inferior direction) was 9 cm for the phantom study. The accuracy of dose calculation was verified by measurement using an I'm*RT* Phantom (IBA Dosimetry GmbH, Schwarzenbruck, Germany); a 0.6-cc Farmer-type ionization chamber, model TN30013 (PTW, Freiburg, Germany); and Gafchromic EBT2 film (International Specialty Products, Wayne, NJ).

For calculation, the I'm*RT* Phantom's electron density was considered equivalent to that of water, and the measured values were corrected using a solid phantom-to-water dose conversion factor (21). Point dose in the phantom was measured at nine points, namely the center of the phantom and points shifted vertically and horizontally by ±3 cm (Fig. 1A). To investigate the dose distribution of MV-CBCT alone, Gafchromic film in the I'm*RT* Phantom was irradiated ten times. To simulate clinical use, films were irradiated with MV-CBCT, as well as the series of IMRT beams from one patient. The summed dose distribution was analyzed. For analysis of radiochromic films, three-channel data (red-green-blue) were acquired at 150 dpi, using a flatbed scanner (model ES-10000G; Epson Seiko Corp., Nagano, Japan). We used software developed inhouse to extract red channel data from scanned images and converted them to dose distribution data, using dose calibration curve prepared for EBT2 films. We confirmed that the difference in responses of EBT2 film to 6 MV and 10 MV X-radiation was negligibly small (data not shown), and therefore, we used the calibration curve prepared using 10 MV X-rays for the analysis of films. The planar dose maps extracted from films and exported from XiO were imported into MapCHECK version 5.01.02 software (Sun Nuclear, Melbourne, FL), and the differences between dose distribution measured by films and that calculated by XiO were evaluated using the γ index (22).

Patients and IMRT planning

We retrospectively analyzed the treatment plans of 22 patients with intermediate- or high-risk prostate cancer, who were treated with IMRT between March and November 2009. A radiation oncologist delineated the prostate and seminal vesicles of all patients. The clinical target volume (CTV) was generated for the prostate and part of the seminal vesicles, and the overlapping region of the CTV with margins for all directions and rectum was then subtracted and defined as the planning target volume (PTV).

OARs were contoured by medical physicists and reviewed by a radiation oncologist. Bladder and rectal volumes were defined as solid structures within the external organ contour. The rectum was delineated from the rectosigmoid junction to the level of the ischial tuberosity or the anus. The prescribed dose was 74 Gy/37 fractions. PTV and OAR volume information for the patients is listed in Table 1. A five-field coplanar treatment plan with beam angles of 45°, 105°, 180°, 255°, and 315° was generated using a 10-MV photon beam for each patient. After optimization, the final dose was calculated using a fast Fourier transform convolution algorithm with a grid size of 2.0 mm.

Imaging dose integration and reoptimization of the IMRT plan

For all patients' IMRT plans, the dose covering 95% of PTV (D95) was normalized to the prescribed dose (74 Gy). To create simple addition plans, an arc beam mimicking 6-MV CBCT was added to the clinically approved treatment plan of each patient. The craniocaudal CBCT imaging range was 10 cm. The D95 value from total beams clearly exceeded the prescribed dose.

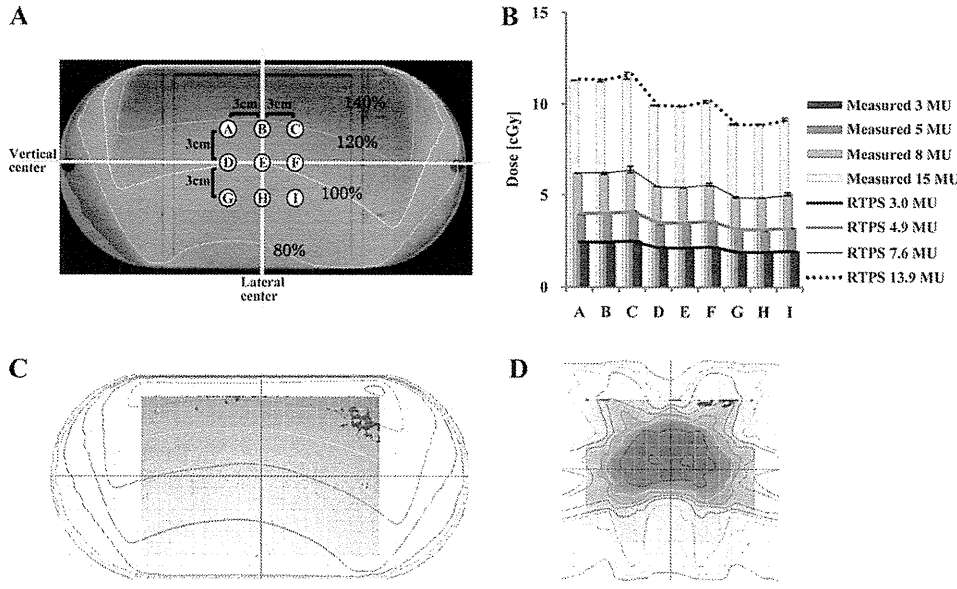

Fig. 1. (A) Dose distribution of MV-CBCT and location for measurement of point-dose using an ion chamber is shown. The axial plane of the I'm*RT* Phantom, displaying measurement points, is shown. Isodose lines show relative dose to the isocenter as calculated by using a XiO system. (B) MV-CBCT dose comparisons between measurements and calculations are shown. The horizontal axis corresponds to the location in panel A. Columns and bars represent means ± standard deviations (SDs) for measurements. The lines indicate the calculated values. The γ analysis using EBT2 film for (C) 15-MU CBCT alone and (D) IMRT beams with 3-MU CBCT of a representative patient is shown. The criterion of γ analysis is 3%/3 mm, and the region exceeding the criterion is red. The dose distributions of films and calculations are shown as gray-scale and lines, respectively.

Two further treatment plan types were created, one involving an additional round of IMRT-beam optimization (reoptimization plans) and a second without this additional optimization (compensation plans). To create compensation plans, the total dose was normalized to D95 by simple rescaling of IMRT beam weights, keeping imaging doses constant. For reoptimization plans, another optimization was performed after adding MV-CBCT. The dose constraints for reoptimization were not altered from the clinically approved treatment plans to eliminate any differences with regard to planner's individual techniques. After optimization, PTV D95 was normalized to the prescribed dose.

To assess the effects of daily portal imaging without incorporating imaging dose into the prescribed dose, two orthogonal beams mimicking portal imaging beams were created in the RTPS. The energy, field size, and imaging MU values for the portal imaging beams were 6 MV, 15 × 15 cm^2, and 1 MU, respectively, for both anterior-posterior and lateral beams. Total numbers of fractions were equal for portal imaging and IMRT. Dose calculation accuracy, linearity, and repeatability for X-ray beams with small MU were verified monthly.

Plan evaluation

To evaluate target coverage quality, PTV homogeneity (*HI*) and conformity (*CI*) indices were calculated using the following formulas:

$$HI = D_{\max}/D_{\min}$$

and

$$CI = V_{Rx}/V_{PTV}$$

where $D_{\max}$, $D_{\min}$, V_{Rx}, and V_{PTV} represent maximum dose, minimum dose, prescription isodose volume, and the PTV volume, respectively. *HI* represents the increase or decrease of hot and cold regions. The values are close to unity for homogenous plans and are large for inhomogeneous plans. *CI* stands for plan conformality. In this study, PTV D95 was normalized to the prescribed dose and was never changed by compensation and reoptimization. *CI* therefore stands for the ineffective dose delivered around PTV. *CI* values are close to unity for conformal plans and become larger for nonconformal plans.

For OARs, rectal and bladder mean doses (D_{mean}) were calculated as follows:

$$D_{mean} = \sum_i \frac{D_i V_i}{V}$$

where V_i is the volume receiving a certain dose (D_i), and V stands for total volume. To evaluate the variations of radiobiological effects from the imaging dose, the generalized equivalent uniform dose (gEUD) proposed by Niemierko (23) for each OAR was also calculated, as follows:

$$gEUD = \left(\sum_i \frac{V_i}{V} D_i^{1/n} \right)^n$$

where n is a parameter that describes the volumetric dependence of the dose-response relationship for each organ. When n = 1, the

Table 1. Patient information and calculated dose of MV-CBCT for each patients

	Volume (cc)			MV-CBCT dose (cGy)			
Dose	PTV	Rectum	Bladder	3 MU	5 MU	8 MU	15 MU
Median	71.9	42.4	132.9	80.8	131.9	204.6	374.1
Minimum	52.9	28.8	23.2	77.1	125.9	195.3	357.1
Maximum	136.9	61.3	363.0	85.4	139.6	216.5	395.9

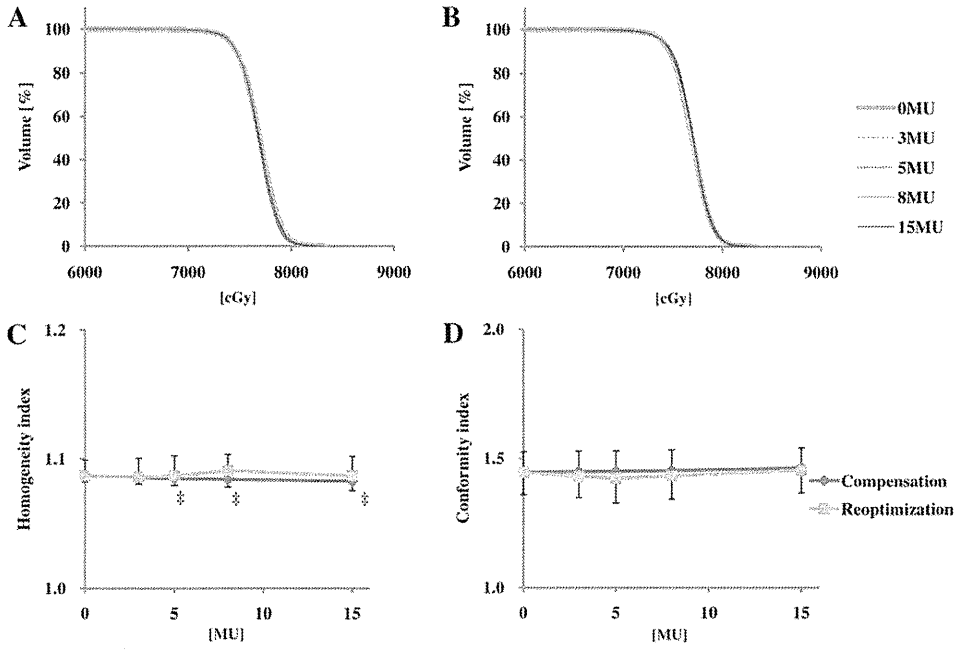

Fig. 2. Evaluation of the effects of MV-CBCT integration and reoptimization of PTV dose coverage. Representative DVHs for (A) compensation plans and (B) reoptimization plans are shown. PTV homogeneity (C) and conformity (D) indices are shown: imaging-MU is plotted along the x-axis and points and bars represent median and interquartile ranges, respectively. †, $p < 0.05$; ‡, $p < 0.01$. (Paired *t*-tests show a comparison between compensation and reoptimization plans with the same MU).

gEUD value is equal to D_{mean}, and a lower n value indicates stronger high-dose sensitivity. The gEUD represents the homogeneous dose distribution that results in the same probability of complications as that of an inhomogeneous dose distribution. The values of n were 0.12 and 0.5 for rectum and bladder, respectively, as Burman et al. previously reported (24). The rectal and bladder volumes receiving a certain dose (Vx) were also analyzed. For calculating D_{mean}, gEUD, and Vx, the dose-volume data were derived from dose-volume histogram (DVH) data exported from RTPS.

Statistical analyses

Statistical significance was assessed using the paired *t*-test, and statistical significance was set at a p value of <0.05. The Bonferroni correction was used for multiple comparison.

RESULTS

MV-CBCT dose calculation accuracy

The monitor chamber mounted on the LINAC indicated values (actual MU) of 2.7 ± 0.0, 4.5 ± 0.0, 7.2 ± 0.0, and 13.3 ± 0.1 MU for MV-CBCT beams with set MU of 3, 5, 8, and 15 MU, respectively. In a preliminary study using actual MU for calculations, unacceptable calculation errors (>10%) were observed, particularly for low-MU CBCT, although the treatment arc beam was calculated accurately (data not shown). In our study, the imaging MU values for calculations were determined by conforming the calculated dose to the dose measured using the ionization chamber. The doses from MV-CBCT for 3, 5, 8, and 15 MU (set MU) measured at the center of I′m*RT* Phantom corresponded to 3.0, 4.9, 7.6, and 13.9 MU, respectively, determined by using the XiO system. MV-CBCT doses measured by the ionization chamber and calculated by the RTPS are compared in Fig. 1B. For all eight points around the center of the I′m*RT* Phantom (Fig. 1B, point E), the error between the measured and calculated doses was less than 1.3% for all imaging MU, and the maximum absolute error was 0.08 cGy.

We also assessed MV-CBCT dose distribution calculation accuracy along the axial plane in the I′m*RT* Phantom (Fig. 1C and D). The criterion of γ analysis is 3%/3 mm, and the region exceeding the criterion was colored red. The CBCT dose distribution agreed well with the calculation (Fig. 1C). To assess the calculation accuracy for clinical use, two-dimensional dose distributions of MV-CBCT combined with IMRT beams were measured using film and compared with the calculation. The representative result using 3-MU CBCT is shown in Figure 1D. Almost all regions passed the criterion for any MU. The pass rate was greater than 98% for CBCT with or without IMRT.

Effect of reoptimization on PTV homogeneity and conformality

Figure 2A and B shows the PTV DVH for compensation and reoptimization plans, respectively. One patient with PTV and OAR volumes close to the median values was chosen. For both techniques, the curves of plans with 3- to 15-MU CBCT were highly similar to those of the nonimaging plan (0 MU), indicating little change in PTV coverage. Figure 2C and D shows PTV *HI* and *CI* indices, respectively. For *HI*, no significant differences were noted for both techniques compared with nonimaging values. Compensation with 5 to 15 MU showed a statistically significant decrease

of *HI* compared to reoptimization, although the amplitude was small. The change in *CI* was not statistically significant for any imaging dose.

Effects of reoptimization on OAR dose

Figure 3A illustrates changes in the rectal D_{mean} value from nonimaging values. While both compensation and reoptimization plans showed an imaging dose-dependent increase in rectal D_{mean}, reoptimization significantly suppressed dose elevation by half compared with compensation ($p < 0.001$ for all MU). Whereas the D_{mean} value of compensation plans became larger than observed with portal imaging when 8- to 15-MU CBCT was added, the D_{mean} value of reoptimization plans did not exceed that of portal imaging. Figure 3B shows the changes in gEUD from nonimaging plans. For the simple addition of portal imaging and 3-MU CBCT, the amplitude of gEUD elevation was similar to that of D_{mean}. In contrast, gEUD determined by both techniques changed modestly with every imaging dose. Because gEUD reflects the effect of inhomogeneous dose distribution, the cause of the disagreement seen in these results may be found in the dose-volume analysis (Fig. 3C). The rectal *Vx* value was uniformly elevated by addition of portal imaging and 3-MU CBCT. In contrast, compensation plans showed a remarkable increase of low-dose volume (V30–V50), while the changes in high-dose volume (V60–V70) were modest. The *Vx* elevations, especially those of low-dose volumes, were suppressed by reoptimization. No significant difference was noted between V60 for compensation and reoptimization plans when 3-MU CBCT was added, and there was no significant difference in V70 for all MU.

Figure 4 shows results for bladder doses subjected to the same analyses as those conducted above. The bladder D_{mean} value was also increased with increasing imaging dose (Fig. 4A). Unlike the results for the rectum, however, gEUD increased significantly for compensation and reoptimization plans compared with nonimaging values (Fig. 4B), and reoptimization significantly suppressed the gEUD elevation when 5 to 15 MU were added ($p = 0.008$ and 0.001 and $p < 0.001$ for 5 and 8 and 15 MU, respectively). As the analysis of *Vx* (Fig. 4C) shows, V70 was increased with increasing CBCT dose, and reoptimization significantly suppressed V70 elevation when 5 to 15 MU

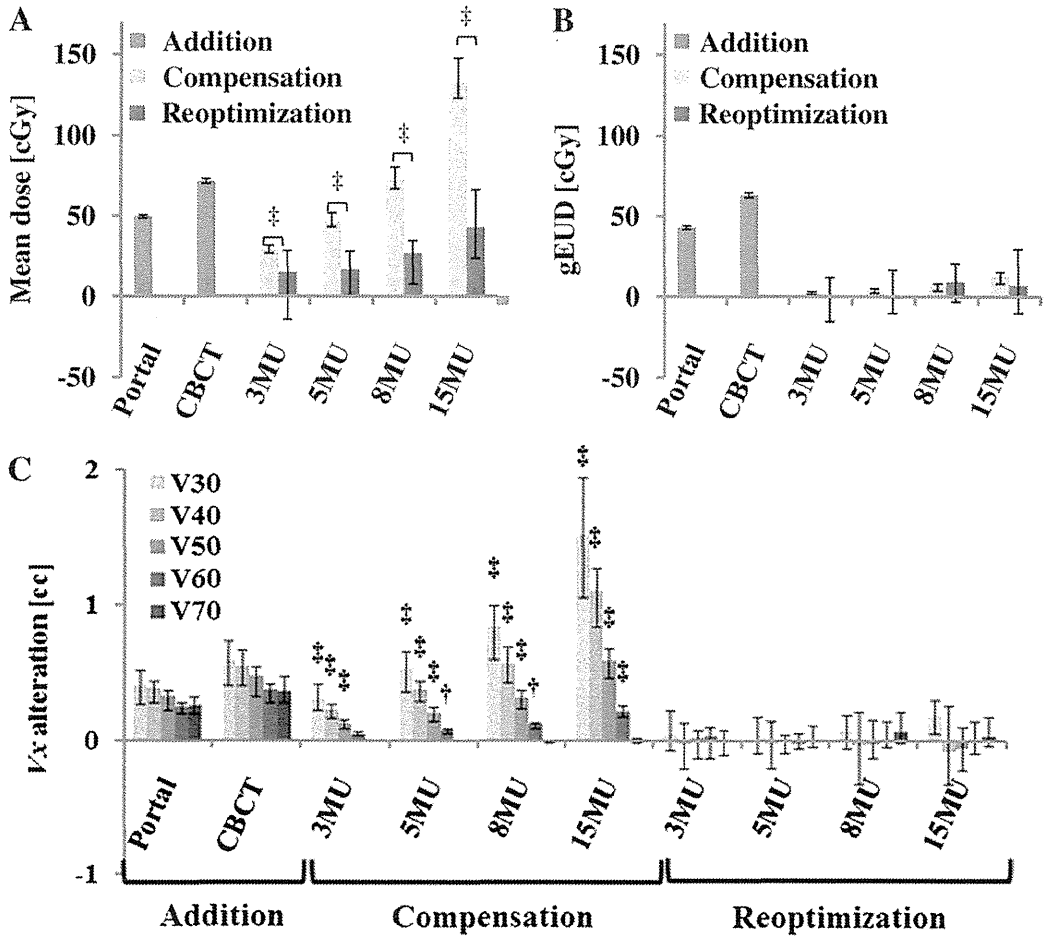

Fig. 3. The effects of MV-CBCT integration on rectal dose. The D_{mean} (A), gEUD (B), and *Vx* (C) values are shown. Each value represents the change from those of nonimaging plans. Columns and bars represent median and interquartile range, respectively. †, $p < 0.05$; ‡, $p < 0.01$. (Paired *t*-test comparisons between compensation and reoptimization plans with the same MU are shown).

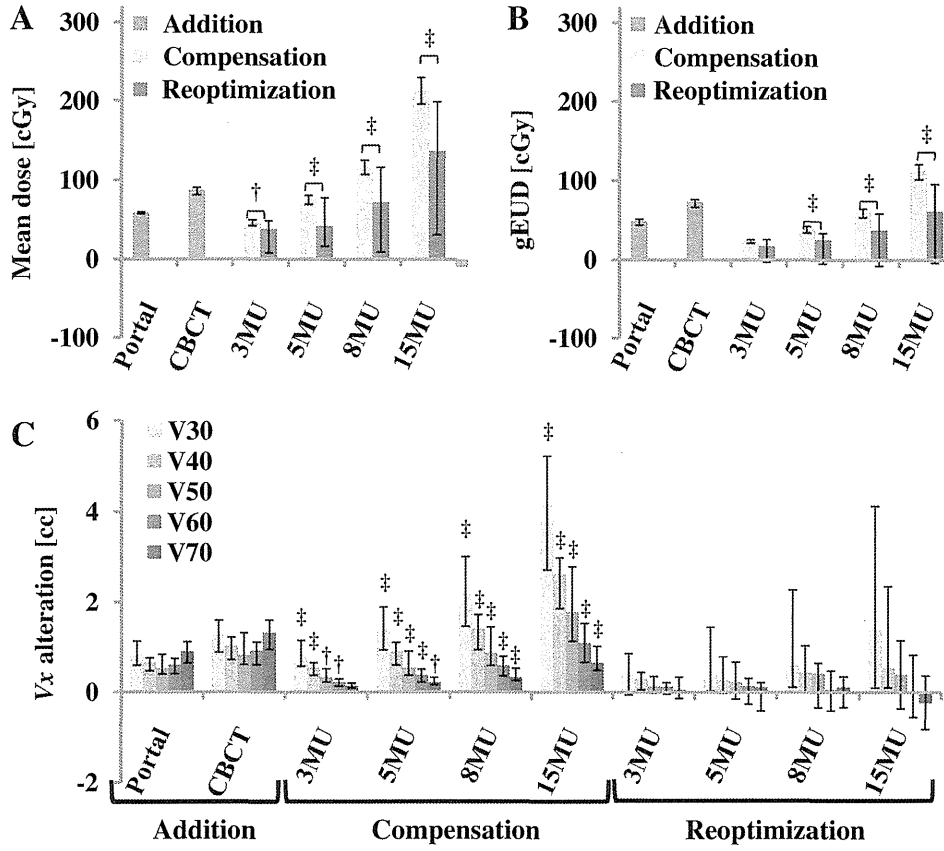

Fig. 4. The effects of MV-CBCT integration on bladder dose are shown. The D_{mean} (A), gEUD (B), and *Vx* (C) values are shown. Each value represents the change from those of nonimaging plans. Columns and bars represent median and interquartile range, respectively. †, $p < 0.05$; ‡, $p < 0.01$. (Paired *t*-test comparisons between compensation and reoptimization plans with the same MU are shown).

were added ($p = 0.044$ and 0.009 and $p < 0.001$ for 5 MU and 15 MU, respectively).

DISCUSSION

The accurate calculation of MV-CBCT dose distribution is essential to the integration of imaging dose with prescribed dose. Here, we were able to accurately calculate MV-CBCT dose distribution by using our method, even for quite low MU (Fig. 1B–D). We confirmed the fact that this method also allowed the accurate calculation of dose in differently shaped phantoms and that the stability of the MV-CBCT beam output was ensured by weekly measurement, routinely performed for IMRT quality assurance. We conclude that our method is feasible for any imaging dose, if the stability of beam output is confirmed by scheduled measurements. Similarly, the report of the American Association of Physicists in Medicine Task Group 142 recommended annual or more frequent assessment of imaging dose (25).

Regarding target coverage, compensation plans showed slightly decreased *HI* (Fig. 2C), indicating a decrease in hot or cold regions in the target volume. This is attributed to the uniform dose distribution of the MV-CBCT dose. However, the alteration was quite small and might be considered clinically negligible. Because the results of *HI* and *CI* demonstrated that MV-CBCT dose integration with both techniques did not worsen the quality of target coverage, the necessity of reoptimization can be simply evaluated by considering the effects of imaging dose on critical organs.

For the rectal D_{mean} value, reoptimization seemed to have a significant advantage for suppressing rectal dose elevation upon addition of imaging dose, particularly for high-MU CBCT (Fig. 3A). However, gEUD values for both techniques showed negligible changes from nonimaging values (Fig. 3B). The results of dose-volume analysis (Fig. 3C) explain the cause of the disagreement: compensation plans mainly increased low-dose volume (30–50 Gy), while their alteration of high-dose volume was modest. In contrast, simple addition of both portal imaging and 3-MU CBCT uniformly increased rectal *Vx*. In general, rectal complications result from high doses (26). Although many studies have demonstrated the association of late rectal toxicity with high dose (≥60 Gy), rectal bleeding correlates with the volume exposed to intermediate doses (40–60 Gy) (26, 27). Jackson et al. (27) stated that the intermediate dose might be associated with the recovery of tissue exposed to high dose. While compensation might be sufficient for reducing rectal injury, reoptimization could still be beneficial for reducing the volume receiving intermediate dose.